The effects of solvents on the modification of SAPO-34 zeolite using 3-aminopropyl trimethoxy silane for the preparation of asymmetric polysulfone mixed matrix membrane in the application of CO$_2$ separation

M.U.M. Junaidi, C.P. Khoo, C.P. Leo *, A.L. Ahmad

School of Chemical Engineering, Universiti Sains Malaysia, Engineering Campus, Seri Ampangan, 14300 Nibong Tebal, S.P.S., Pulau Pinang, Malaysia

ARTICLE INFO

ABSTRACT

SAPO-34 zeolite is the ideal porous filler in Mixed matrix membranes (MMMs) for CO$_2$ separation because it has strong affinity towards CO$_2$ and pore size (0.38 nm) which is nearly similar to the molecular sizes of various gasses in natural gas. However, the poor compatibility between zeolite and polymeric matrix causes the formation of non-selective interfacial voids, leading to poor separation of gasses. In this work, 3-aminopropyl trimethoxy silane (APMS) was proposed to modify SAPO-34 zeolite before adding into asymmetric polysulfone (PSf) MMMs prepared via dry–wet phase inversion. The effects of solvent (ethanol or isopropanol) in grafting reaction were studied. The changes in FTIR spectra of both modified SAPO-34 zeolite samples signified that more silane molecules were grafted when ethanol was used. SAPO-34 zeolite dispersed evenly in PSf matrix after modification as shown in EDX analysis. Although showing similar FTIR spectra and morphology, a great improvement in CO$_2$ selectivity and permeance was only shown by PSf/SAPO-34E MMMs with zeolite modified using APMS in ethanol. The highest CO$_2$/N$_2$ selectivity of 28, CO$_2$/CH$_4$ selectivity of 31 and a satisfactory CO$_2$ permeance of 706 GPU were achieved. Besides reduction of filler agglomeration, the improvement could be related to the diminished interfacial voids when SAPO-34 zeolite was modified using APMS in ethanol.

© 2013 Elsevier Inc. All rights reserved.

1. Introduction

Zeolites are inorganic aluminosilicate materials which have shown great potential in membrane gas separation due to their well-defined repeating pore structures. The accurate size and shape discrimination resulted from a narrow pore distribution ensures the superior selectivity in gas separation [1]. SAPO-34 zeolite is particularly suitable for gas separation because its chabazite (CHA) structure has a 0.38 nm framework pore size; which is nearly similar to the molecular sizes of various gases, especially in a natural gas application. Thus, SAPO-34 zeolite has been added as the selective fillers in mixed matrix membranes (MMMs) for carbon dioxide (CO$_2$) separation [2,3]. In general, MMMs composed of polymer as the continuous phase and inorganic filler as the dispersed phase. MMMs exhibit the combined superior properties of both inorganic fillers and polymer to achieve excellent gas separation performance [4]. However, non-selective interfacial voids form in the MMMs due to the poor compatibility between the polymer and inorganic fillers, resulting profound impact on the

separation performance [5]. Silane coupling agents were commonly proposed to improve the compatibility of zeolite in polymeric matrix. Silane coupling agents are silicon-based chemicals which contain two types of reactive groups, namely inorganic and organic groups in the same molecule. The general formula of a silane coupling agent is R-(CH$_2$)$_n$-Si-X$_3$ in which X is a hydrolyzable group, such as methoxy, ethoxy or acetoxy, while R is an organo functional group, such as amino, methacryloxy and epoxy. After grafting on the zeolite, the silane coupling agent acts as an effective interface, which is a complex interaction of chemical and physical factors, such as concentration gradient, expansion coefficient and adhesion. The unique physical and chemical properties of silane coupling agent can even prevent debonding during composite aging [6].

Pechar et al. [7] reported the use of 3-aminopropyltrimethoxysilane (APTMS) to modify ZSM-2 zeolite before blending into polyimide membranes. Although SEM and TEM micrographs showed the absence of voids, the MMMs showed poor performance in terms of CO$_2$ selectivity and permeability due to the pore blockage on ZSM-2 zeolite [8]. Pechar and co-workers further used silanated zeolite L filler modified with 3-aminopropyltriethoxysilane (APTES) to prepared polyimide MMMs. Both CO$_2$ selectivity and

---

* Corresponding author. Tel.: +60 4 5996425; fax: +60 4 5941013.
  E-mail address: chcpleo@eng.usm.my (C.P. Leo).

permeability of the modified MMM dropped relatively to the neat membrane. The reduction of CO_2 adsorption indicated the zeolite pores was also partially blocked by APTES. Instead of using toluene as the solvent in the silane modification, Ismail et al. [6] modified zeolite 4A using APTES in ethanol. Besides the good compatibility between the modified zeolite and polyethersulfone (PES) membrane was observed, a great improvement in the CO_2 selectivity was achieved. However, the CO_2 permeability was reduced nearly 80% compared to the neat PES membrane. The reduction of permeability can only be explained by the polymer rigidification [9].

In the preparation of PES MMMs, Li et al. [10] modified zeolite 3A, 4A and 5A using 3-aminopropylmethyldiethoxy silane (APMDES) in toluene. The modification reduced the rigidification of polymer chain and partial pore blockage which induced by the polymer matrix. As a result, both of the selectivity and permeability of CO_2 via MMM blended with the modified zeolite were higher than those MMMs containing zeolite without the modification. Similar improvement in the gas separation was reported by Hillock et al. [9] who fabricated MMMs using SSZ-13 zeolite modified with (3-aminopropyl)-dimethyl-ethoxysilane (APDMES) in toluene as well. A group of researchers from Laval University [11], also synthesized 6FDA-ODA MMMs using intergrowth Faujasite and EMC-2 (FAU/EMT) zeolite grafted with APMDES. They reported that MMMs with 25 wt.% of zeolite grafted at optimum grafting condition (85 °C, 24 h and 0.35 mmol APMDES/ml isopropanol (IPA)) exhibited great improvement in both CO_2 selectivity and permeability compared to the neat polyimide membrane. However, modified MMMs possessed lower permeability, but higher selectivity as compared to unmodified MMM. Increasing the amount of APMDES chained on zeolite structure resulted rigidified interfacial phase [11]. Additionally, the reduction of surface area and micropore volume of the zeolites suggested the zeolite pores were also partially blocked by the silane coupling agent. In their subsequent study [5], FAU/EMT zeolite was grafted with APTES, APMDES and APDMES in solvents with varied polarity. The result revealed that all the modified MMMs, especially those MMMs containing modified zeolite using APTES with IPA as the grafting solvent, possessed higher CO_2 selectivity and permeability compared to the unmodified MMMs and neat polymeric membranes. Besides improving filler/polymer interface, the grafting reaction further prevented the filler sedimentation, yielding improved homogenous dispersion of zeolite particles in polymeric matrix. The employment of polar solvent, such as IPA, in grafting reaction could generate more uniform distribution of grafting sites by increasing mobility of the aminosilane molecules. In addition, BET surface area was not much affected by changes on the amount of grafted aminosilane.

To our best knowledge, not much research work focuses on the silane modification of SAPO zeolites to prepare MMMs for CO_2 separation. Based on the detailed literature review, modification of SAPO zeolite using silane has a great potential to further enhance the CO_2 separation of MMMs. In this work, 3-aminopropyl trimethoxy silane (APMS) was selected as silane coupling agent because methoxy silanes are more readily in hydrolysis reaction compared to ethoxy groups [12]. In addition, the effects of IPA and ethanol as the solvent for silane grafting were compared in order to achieve satisfactory CO_2 separation.

2. Experimental

2.1. Synthesis, modification and characterization of SAPO-34 zeolite

SAPO-34 zeolite was prepared as reported by Li et al. [13]. A gel with molar composition of Al_2O_3:P_2O_5:0.6 SiO_2:1.0 TEAOH:56 H_2O was prepared by mixing H_3PO_4 (Merck, 85 wt.% aqueous solution),

Al $(i-C_3H_7O)_3$ (Sigma–Aldrich) and deionized (DI) water for 12 h at room temperature. Then, the template solution, tetraethylammonium hydroxide (TEAOH) (Sigma–Aldrich, 35 wt.% in aqueous solution) was added into the mixture and stirred for 30 min. After stirring, the colloidal silica sol (Ludox AS4, 40 wt.% in aqueous solution) was added and the solution was stirred vigorously for 18 h. Then, the solution was transferred into the stainless steel parr reactor for hydrothermal synthesis at 200 °C for 24 h. Upon completion of synthesis, the sediments which contained zeolite crystals were washed using DI water and centrifuged for several times before being dried in a oven for 24 h at 100 °C. The dried zeolite crystals were then calcined at 500 °C for 5 h to remove the template from the zeolite framework.

In the silane modification preparation, the reaction solution was planned according to literatures [14,15]. 0.1 ml of APMS (Merck) was hydrolyzed by mixing with the mixture of solvent (IPA (Merck) or ethanol (Merck)), DI water and hydrochloric acid (HCl, fuming 37%, Merck) with a volume ratio of 19 solvent:H_2O:0.02 HCl. The solution was stirred for 15 min at room temperature. SAPO-34 zeolite modified using APMS in IPA solution was designated as SAPO-34I while SAPO-34 zeolite grafted using APMS in ethanol solution was designated as SAPO-34E. Then, 1 g of dried SAPO-34 zeolite was added into the hydrolyzed solution and stirred for 40 min at 50 °C. The solution was transferred to petri dish and left in fume hood overnight to evaporate off the volatile solvent. Then, the solution was then placed in oven to remove excess water trapped inside SAPO-34 zeolite.

X-ray diffraction (XRD) analysis was conducted using a diffractometer (Bruker AXS D8 Advance 61, Germany) to identify the crystal structure of SAPO-34 zeolites. The system was equipped with a Cu X-ray tube (18 kW C Kα radiation; λ = 0.15418 nm) and a LynxEye detector operated in the theta–theta geometry at 60 kV and 80 mA. Scanning was performed from 5° to 35° (2θ) with a step width of 0.02° and a sampling time of 0.3 s per step. The zeolite samples were characterized using a Fourier Transform Infrared (FT-IR) spectrometer (Nicolet iS10, Thermo Scientific, USA) as well
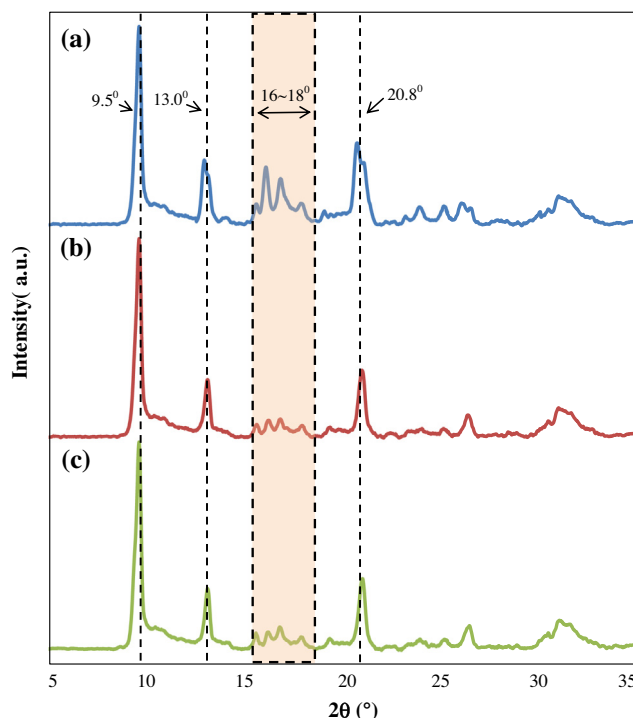

Fig. 1. X-ray diffraction patterns of (a) SAPO-34, (b) SAPO-34E and (c) SAPO-34I.
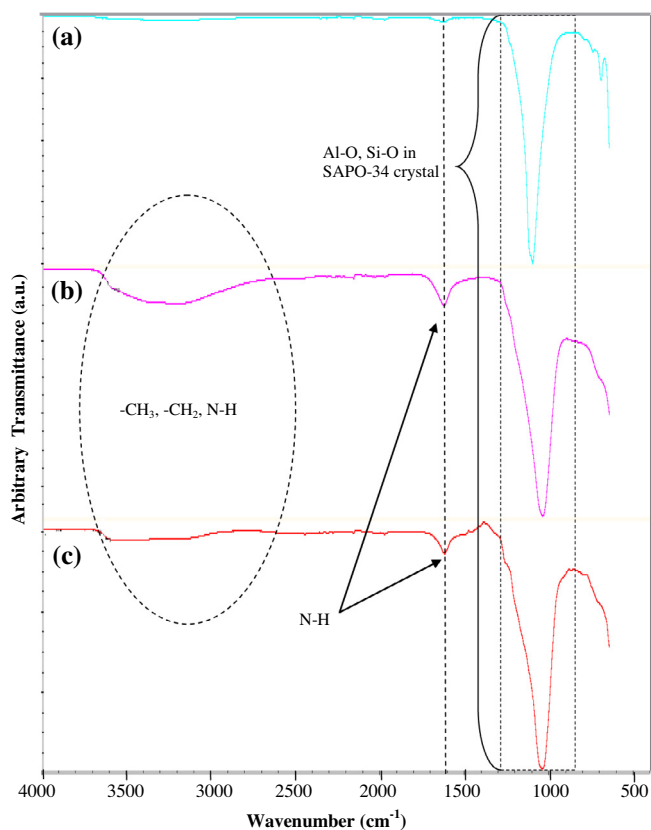
Fig. 2. FTIR spectra of (a) SAPO-34, (b) SAPO-34E and (c) SAPO-34I.

Table 1
BET characterization data.

Zeolite	BET surface area (m²/g)	Pore volume (cm³/g)	Reference
SAPO-34	535	0.24	[16]
SAPO-34	498	0.25	This work
SAPO-34E	492	0.24	This work
SAPO-34I	331	0.15	This work

to determine the possible functional groups and amine-functionalized grafting present in SAPO-34 zeolite. All FTIR spectras were obtained with 32 scans at 4.00 cm⁻¹ resolution. The surface area and pore volume of the calcined zeolite samples were obtained by the N_2-dynamic adsorption/desorption technique using a Micromeritics ASAP 2020. The surface area was calculated using Brunauer–Emmett–Teller (BET) method while the pore volume was calculated using *t*-Plot micropore method.

2.2. Synthesis and characterization of PSf membrane and PSf/SAPO-34 MMMs

SAPO-34 zeolites and polysulfone (PSf) pellets (Sigma–Aldrich, MW ∼35,000) were dried in an oven at 120 °C for 24 h. The neat PSf casting solution consisted of 25 wt.% of PSf, 47 wt.% of 1-methyl-2-pyrrolidinone (NMP, Merck), 18 wt.% of tetrahydrofuran (THF, Reidel-de Haën) and 10 wt.% ethanol. The PSf pallets and ethanol were mixed in the NMP-THF solution at ambient temperature for 5 h. MMMs solutions were prepared by first stirring 10 wt.% SAPO-34 zeolite crystal (SAPO-34, SAPO-34E or SAPO-34I) in NMP–THF–ethanol solution for 2 h and then sonicating for 15 min. Then, PSf was added into the solution and mixed for 1 day. Prior to the casting, the solution was degassed for 2 h to

eliminate the micro-bubbles trapped inside the solution. Membranes were prepared via dry–wet phase inversion method. The casting solution was poured onto a clean flat glass plate to form thin layer which is formed using a casting knife with 0.2 mm gap at ambient temperature. The solution was left for 90 s for dry step and then was immersed in coagulation bath to form flat sheet membrane which was left overnight. The fabricated membrane was solvent-exchanged with methanol (Merck) for 2 h and followed by drying in oven at 100 °C for 1 day.

Besides FTIR scanning on the membrane samples as stated earlier, Scanning Electron Microscope (SEM) (Quanta FEG 450 Oxford Instrument, Netherlands) was used to observe the top surface and cross section morphology of the membranes. All membrane samples were fractured using liquid nitrogen prior scanning. The membrane samples were mounted on the sample holders and observed under high vacuum condition at potentials of 10.0 kV.

2.3. Gas permeation measurement

The single gas permeation test was carried out for every membrane sample using CO_2, N_2 and CH_4 gasses with more than 99% purity. Gas permeation test was carried out at ambient temperature and a feed pressure of 4.48 bar. Flat sheet membrane discs with a diameter of 4 cm and effective membrane area of 12.6 cm² were tested. Soap bubble flow meter was used to measure the volumetric flow rate of permeated gas. Each set of the measurement data represents an average of 3 replicates. The unit for gas permeation measurement used is Gas Permeation Unit (GPU), where 1 GPU is equal to 10^{-6} cm³ (STP)/cm² s cmHg. The ideal selectivity for CO_2/N_2 and CO_2/CH_4 gases was determined from the ratio of gas permeances.
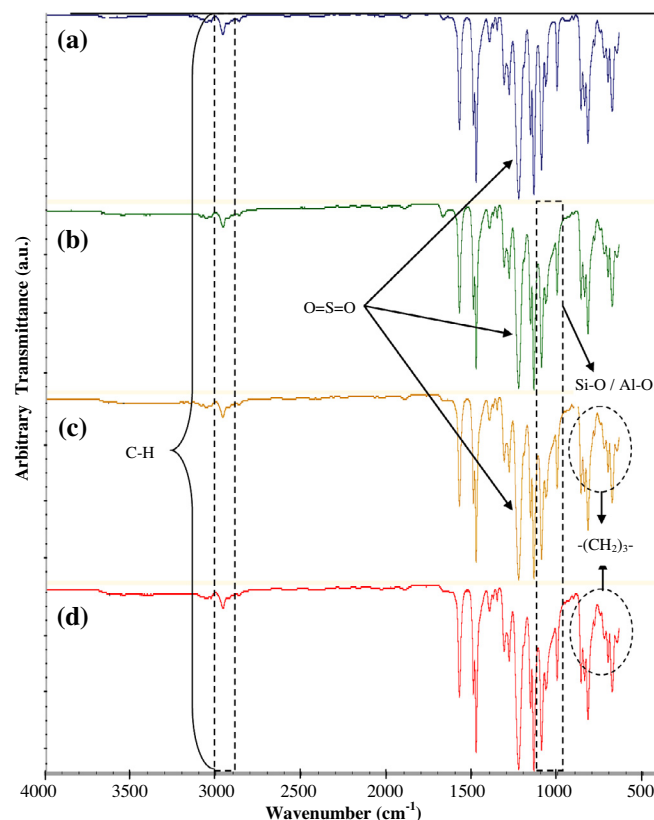

Fig. 3. FTIR spectra of (a) PSf membrane, (b) PSf/SAPO-34 MMM, (c) PSf/SAPO-34E MMM and (d) PSf/SAPO-34I MMM.

3. Results and discussion

3.1. Characterization of unmodified and APMS modified SAPO-34 zeolites

XRD patterns of SAPO-34 zeolites before and after silane modification using different solvents are presented in Fig. 1. All samples exhibited almost identical characteristic peaks, which was corresponded to the CHA structure of SAPO-34 zeolite [16]. Generally, SAPO-34 zeolite samples possessed a major peak at roughly 9.5°, corresponding to a (110) reflection with the highest intensity. Few important minor peaks at 13°, 16.1°, and 20.8° were also identified along with the major peak at 9.5° to confirm the high crytallinity degree of the CHA structure in unmodified and modified SAPO-34 zeolites [17]. Using either ethanol or isopropanol as the solvent during silane modification resulted a reduction of peak intensity in the range of 16–18° as shown by SAPO-34E and SAPO-34I particle samples. The crystalline structure of the SAPO-34 zeolite may be slightly disrupted during the introduction of APMS, resulting in a slight decrement of crystallinity.

FTIR spectra of unmodified SAPO-34 and two modified SAPO-34 samples are shown in Fig. 2. All the FTIR spectra showed great vibration in the range of 850–1200 cm^{-1}. This strong adsorption band indicated the internal tetrahedral asymmetric of Al–O or Si–O group in the SAPO-34 crystal [14]. The FTIR spectra of modified SAPO-34 crystals showed increasing intensity and broadness of band ranging from 3600 cm^{-1} to 2800 cm^{-1} as compared to unmodified SAPO-34 crystal. There were several overlapping bands (i.e. –OH, N–H, Si–OH, –CH$_3$, –CH$_2$) fell in this region [8]. The increment of intensity and broadness of the band at 3370 cm^{-1} and 3290 cm^{-1} was corresponded to N–H stretching vibration in silane, indicating the presence of APMS. Furthermore, the adsorption peaks at 2950 cm^{-1} was related to aliphatic C–H, –CH$_3$ and –CH$_2$ stretching vibrations [6,18]. The intensity of this peak was increased relatively upon the introduction of the silane onto the SAPO-34 as each APMS molecule contained three –CH$_3$ and –CH$_2$ groups, respectively. The N–H bending vibration of typical primary amine was also noticeable at the wavenumber of 1620 cm^{-1} in both modified SAPO-34 crystal samples (SAPO-34E and SAPO-34I), but this peak was absence in the FTIR spectrum of unmodified SAPO-34 crystal. In addition, the characteristic band of the SAPO-34 was shifted from 1104 cm^{-1} to 1046 cm^{-1} after silane modification. This particular shifting of the absorbance peak to lower wavenumber signified qualitatively the interaction between the coupling agent (APMS) and SAPO-34 zeolite to form Si–O–C linkages. Analogous observation was reported by Clarizia et al. [19] when they utilized aminopropyl-diethoxymethyl silane (APDEMS) to modify NaA(LTA) zeolite. In addition, the increment of the intensity of peaks within the range of 750–680 cm^{-1} for both modified SAPO-34 crystals were noticeable due to the various rotations and vibrations within –(CH$_2$)$_3$– group. Therefore, the presence of the –(CH$_2$)$_3$– group could further confirm the existence of APMS on the SAPO-34 surface. Analogous observation was reported by Wahab et al. [20] in the grafting of zeolite 4A using APTES. Comparing
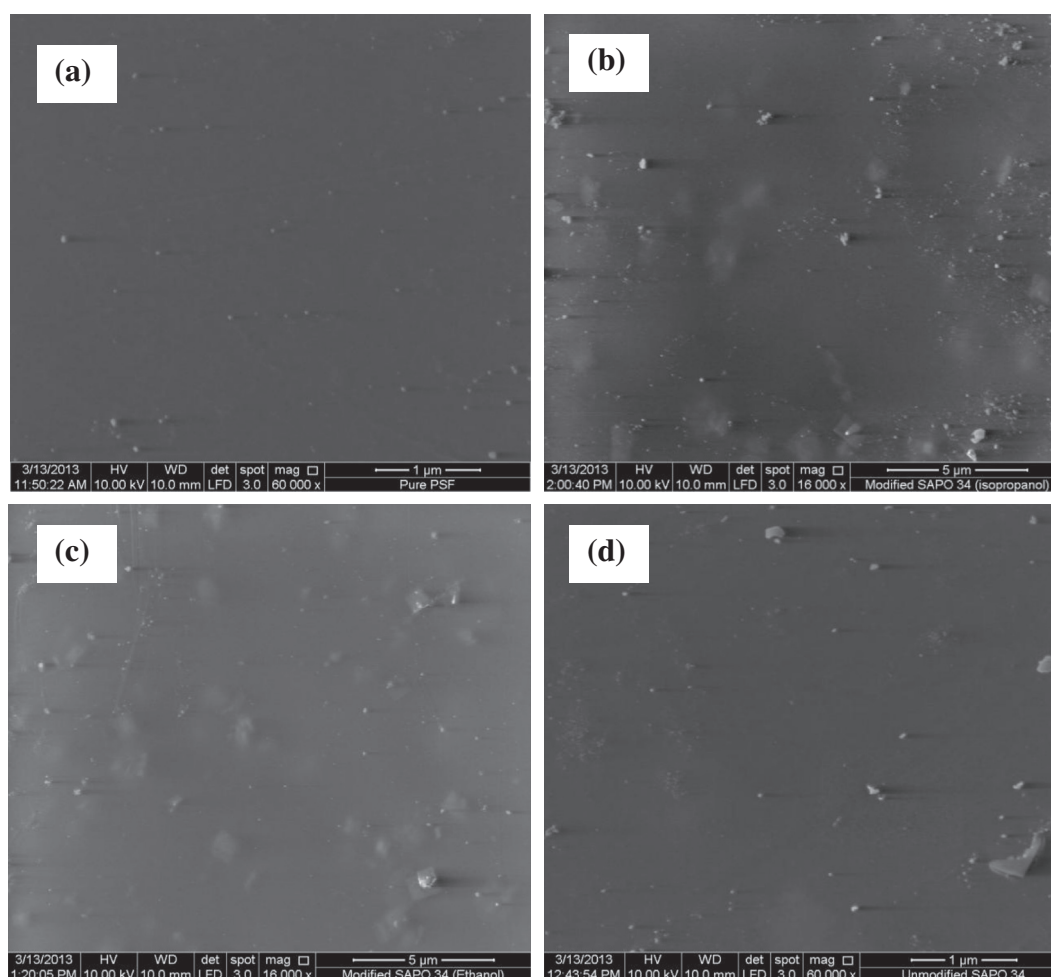

Fig. 4. SEM images on the surface of (a) PSf membrane, (b) PSf/SAPO-34 MMM, (c) PSf/SAPO-34E MMM and (d) PSf/SAPO-34I MMM.

the modified samples, SAPO-34E showed greater intensity at both 1620 cm^{-1} and $3600–2800 \text{ cm}^{-1}$ regions as compared to SAPO-34I. The difference simply signified that more APMS molecules were effectively presented on the SAPO-34 zeolite surface using ethanol as the solvent in grafting reaction.

SAPO-34 zeolite with an average particle size of 0.661 μm [21] was used in this work. The surface area and pore volume of the calcined zeolite samples after silane grafting are summarized in Table 1. In this work, unmodified SAPO-34 exhibited BET surface area of $498 \text{ m}^2/\text{g}$, which is slightly lower than the work reported by Chew et al. [16]. However, higher pore volume compared to literature value [16] was recorded, which tend to increase the porosity of the synthesized zeolite [13]. On the other hand, modified SAPO-34E revealed insignificantly lower surface area and pore volume compared to unmodified SAPO-34. Likewise, Nik et al. [11] faced similar reduction in surface area and pore volume of the FAU/EMT zeolite due to the APMDES modification on zeolite surface cause blockage in the zeolite pores. Meanwhile, APMS modification on SAPO-34 using IPA exhibited severe reduction on surface area ($331 \text{ m}^2/\text{g}$) as well as pore volume compared to SAPO-34E and unmodified SAPO-34 fabricated in this work. The pore of SAPO-34 zeolite may be blocked effectively by the modification of APMS using IPA as solvent, resulting in a ruthless diminution of effective surface area and may disrupt gas separation ability. BET analysis clearly described the APMS modification of SAPO-34 using ethanol is more appropriate due to the significant decrement in BET surface area, rather than SAPO-34I, which apply IPA as reaction solvent.

3.2. Characterization of pure PSf membrane and fabricated MMMs

The FTIR spectra of pure PSf membrane, PSf/SAPO-34, PSf/SAPO-34E and PSf/SAPO-34I are shown in Fig. 3. The FTIR spectrum of pure PSf membrane displayed bands at 1290 cm^{-1} and 1325 cm^{-1}, representing the presence of O=S=O stretching vibration. The adsorption peaks at 2960 cm^{-1} and 1380 cm^{-1} were corresponded to C–H stretching and bending vibrations respectively. Meanwhile, the C=C stretching conjugation of benzene rings was detected at 1565 cm^{-1} [22,23]. All the modified and unmodified MMM samples exhibited the analogous and comparable FTIR spectrums to the pure PSf membrane. However, intense peaks were observed in the range of $900–1200 \text{ cm}^{-1}$ and these peaks corresponded to the asymmetric vibration of Si–O or Al–O tetrahedral in the SAPO-34 filler [14,24]. Both modified MMMs (PSf/SAPO-34E and PSf/SAPO-34I) showed higher shoulder band as compared to the unmodified PSf/SAPO-34 MMM in the band region of $1220–600 \text{ cm}^{-1}$. In the range of $760–680 \text{ cm}^{-1}$, the peaks was observed due to the various rotations and vibrations within $-(CH_2)_3-$ group of silane. Meanwhile, the Si–O–C linkage formation contributed into the peak at 1015 cm^{-1}. However, the low concentration of silane (1 wt.%) led to undetectable peaks of C–N stretching and N–H bending vibrations in the FTIR spectrum.

The surface and cross-section of the neat PSf membrane and MMM samples were shown in Figs. 4 and 5. In Fig. 4(a), no voids were noticeable on the surface of the skin layer of the pure PSf membrane. The formation of spongy-like structure of the sublayers
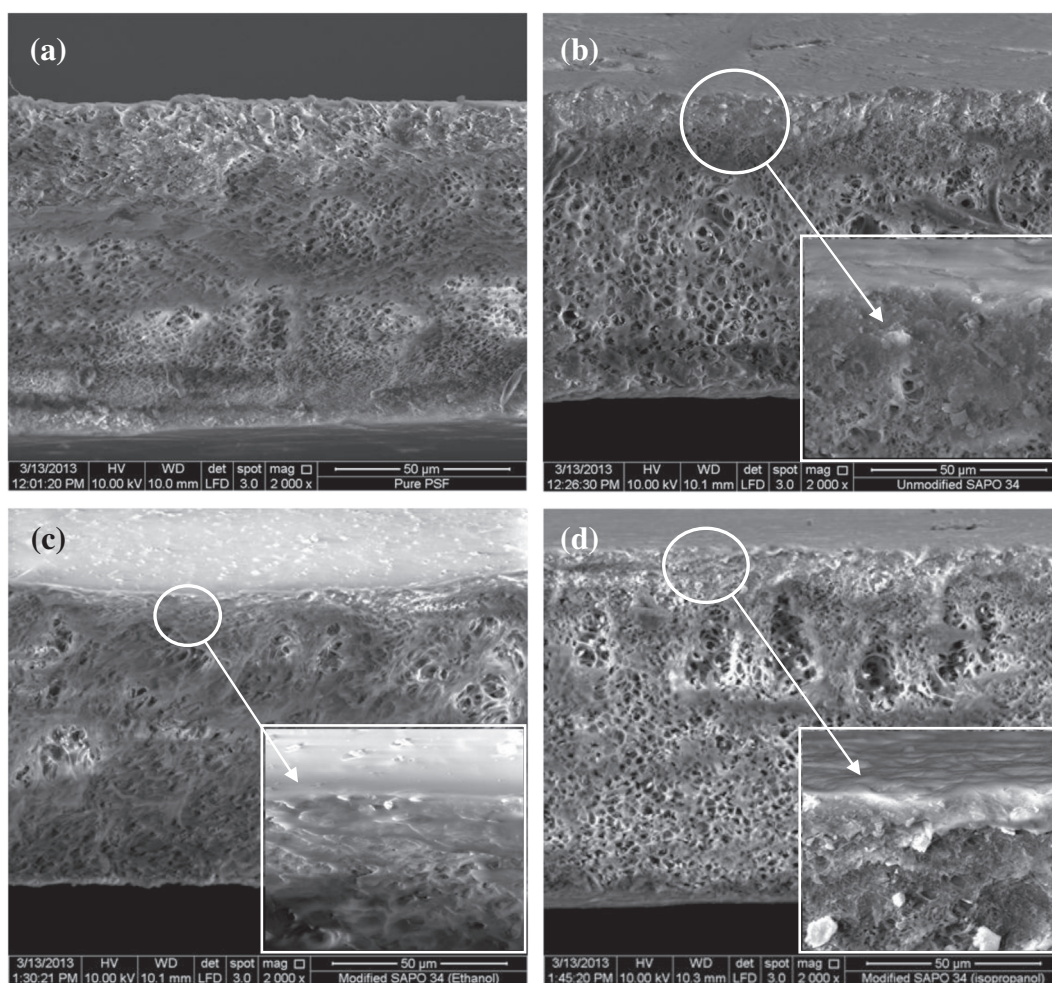

Fig. 5. SEM images on the cross section of (a) PSf membrane, (b) PSf/SAPO-34 MMM, (c) PSf/SAPO-34E MMM and (d) PSf/SAPO-34I MMM.
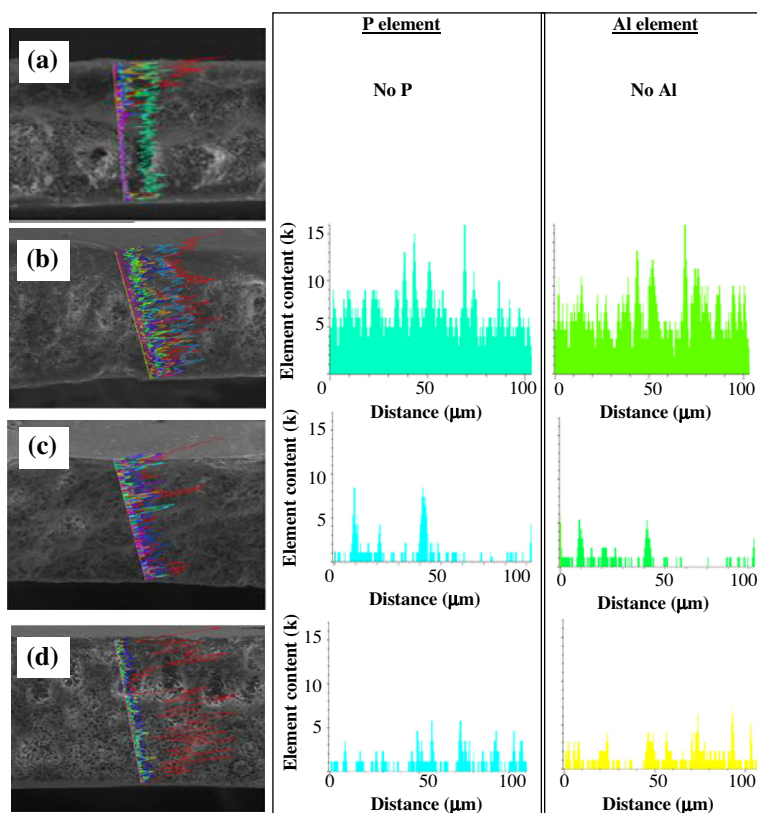
Fig. 6. EDX analysis of (a) PSf membrane, (b) PSf/SAPO-34 MMM, (c) PSf/SAPO-34E MMM and (d) PSf/SAPO-34I MMM.

Table 2
Pure gas permeations/flux and ideal selectivities of pure PSf and MMMs containing unmodified and modified SAPO-34 zeolite.

Membranes	Gas permeance/flux (GPU)			Ideal selectivity	
	CO_2	N_2	CH_4	$\alpha(CO_2/N_2)$	$\alpha(CO_2/CH_4)$
PSf	105	8	7	13	15
PSf/SAPO-34	459	22	17	21	27
PSf/SAPO-34E	706	25	23	28	31
PSf/SAPO-34I	775	35	28	22	28

supporting thin dense skin layer (Fig. 5(a)), was observed and this observation was analogous with other similar work [22,25]. The spongy-like sublayers were mainly contributed by the delayed li-

quid–liquid demixing during phase inversion in the non-solvent bath [26]. Due to the smaller mutual affinity of the solvent and non-solvent and the strong interaction between polymer and polymer [27], the nascent skin layer is formed during the dry-step and would serve as resistance to inhibit the mass transfer of solvents in the casting solution and nonsolvents in the coagulation bath. This phenomena led to the slow permeation of the non-solvent into the casting solution and the precipitation of sublayers proceeded at slower rate. Hence, the spongy-like structure of sublayers were formed [28]. Similar to the neat PSf membrane, MMMs showed the defect-free skin layer on the surfaces as shown in Fig. 4(b)–(d). However, the spongy-like sublayers of MMM samples exhibited slightly larger macrovoid compared to neat PSf sublayers. In addition, the introduction of the modified SAPO-34 into the

Table 3
CO_2 separation performance of asymmetric MMMs reported in recent literatures [20,22,36–40].

Asymmetric membranes	J_{CO_2} (GPU)	$\alpha(CO_2/CH_4)$	$\alpha(CO_2/N_2)$	References
PSf/Silica (0.1 wt.%)	90.04	32.74	–	[20]
PSf/Silica (3 wt.%)	88.06	24.64	–	[20]
PSf/Silica (10 wt.%)	87.69	7.43	–	[20]
PSf/SAPO-44 (5 wt.%)	81.93	25.8	22.3	[22]
PSf/SAPO-44 (10 wt.%)	338.33	10.6	8.2	[22]
PSf/SAPO-44 (20 wt.%)	351.07	1.5	1.2	[22]
Matrimid®/Cu₃(BTC)₂ (3 wt.%)	65	8	6	[36]
Matrimid®/Cu₃(BTC)₂ (6 wt.%)	37	9	6	[36]
Matrimid®/ZIF-8 (10 wt.%)	17	22	25	[37]
Matrimid®/ZIF-8 (20 wt.%)	22	22	25	[37]
Matrimid®/ZIF-8 (30 wt.%)	23	23	27	[37]
Ultem®/ZIF-8 (25 °C)	18	–	44	[38]
Ultem®/ZIF-8 (30 °C)	21	–	39	[38]
Ultem®/ZIF-8 (35 °C)	26	–	36	[38]
Ultem®/ZIF-7	6.2	44	30	[39]
Pebax®/ZIF-7 (8 wt.%)	291	23	68	[40]
Pebax®/ZIF-7 (22 wt.%)	137	30	97	[40]
Pebax®/ZIF-7 (34 wt.%)	39	44	105	[40]

MMM samples possibly induced the thermodynamics instability in the solution, thus led to the rapid phase mixing and larger pore formation [24]. Moreover, the presences of finger-like macrovoids were noticed in PSf/SAPO-34I (Fig. 5(d)). The finger-like macrovoids formation was probably due to the strong interaction of solvent–additive and the weak interaction of solvent–polymer and additive–polymer [29,30]. The unmodified SAPO-34 showed poor interaction with PSf matrix, causing the formation of agglomeration (Fig 5(b)). From the cross-sectional images (Fig. 5(b) and (c)), less agglomeration was formed in the effective skin layer especially PSf/SAPO-34E MMM. The formation of large aggregates could affected the gas performance of MMMs as discussed later.

EDX analysis of a cross sectional line on the pure PSf membrane and MMMs with unmodified or modified SAPO-34 is summarized in Fig. 6. The presence of SAPO-34 zeolites in membrane samples are detected through the existence of Aluminium (Al) and Phosphorus (P) elements in. Except the pure PSf membrane, all the MMMs (PSf/SAPO-34, PSf/SAPO-34E and PSf/SAPO-34I) showed the existence of Al and P elements. Although containing the same filler content, PSf/SAPO-34E and PSf/SAPO-34I MMMs showed much lower P and Al contents compared to PSf/SAPO-34 MMM which contains unmodified fillers. The observation could only be explained by the absence of large agglomerates of zeolite in PSf/SAPO-34 MMM. As observed by other researchers [9], filler agglomerate in polymeric matrix due to the strong electrostatic, steric, and van der Waals forces between particles. Priming is usually used to minimize the agglomeration of zeolite fillers and reduce interfacial defect, while silane coupling agents have proven to reduce interfacial voids in MMMs [9]. Similar to APTES modification [5], APMS even could reduce agglomeration of zeolite in MMMs.

3.3. Gas performance analysis

The gas separation performance of PSf membrane, PSf/SAPO-34, PSf/SAPO-34E and PSf/SAPO-34I MMMs was tabulated in Table 2. The pure PSf membrane exhibited slightly different gas permeation data compared to the literature [22,25], due to the variation in solvent evaporation duration and casting gap. The permeances of all gases via SAPO-34 MMMs were significantly increased, compared to the pure PSf membrane. The increment in N_2 and CH_4 permeation could be related to the presence of interfacial voids. However, tremendous enhancement of CO_2/N_2 and CO_2/CH_4 selectivities up to 71% and 101% respectively was noticed upon the addition of SAPO-34 zeolite. The enhancement could be the contribution of sieving and adsorption effects of SAPO-34 [31,32]. The polar surface of SAPO-34 has great affinity towards CO_2 [33], leading to significant enhancement of CO_2 flux up to 339% as compared to pure PSf in this work. By comparing the recent works reported on MMMs incorporated with SAPO-34 [32,34], the increment of CO_2/CH_4 selectivity in this work is greater which may due to the selection of PSf as the polymeric matrix and the application of asymmetric morphology.

Both types of MMMs with modified SAPO-34 (SAPO-34E and SAPO-34I) showed great enhancement in terms of selectivity and permeation flux relative to the pure PSf membrane in this work as well. The highest CO_2/N_2 and CO_2/CH_4 selectivities were detected in the separation experiments using SAPO-34E MMMs with ethanol as the solvent for silane grafting. The CO_2 selectivity value increased to 28 (135% increment) and 31 (124% increment), respectively, as compared to the pure PSf membrane. SAPO-34E MMMs also showed higher CO_2 selectivity than MMMs with unmodified SAPO-34, by an enhancement of 37.5% for CO_2/N_2 selectivity and 11% for CO_2/CH_4 selectivity. The increment could be related the well dispersion of zeolite as shown in EDX analysis upon the introduction of APMS into the system. The presence of
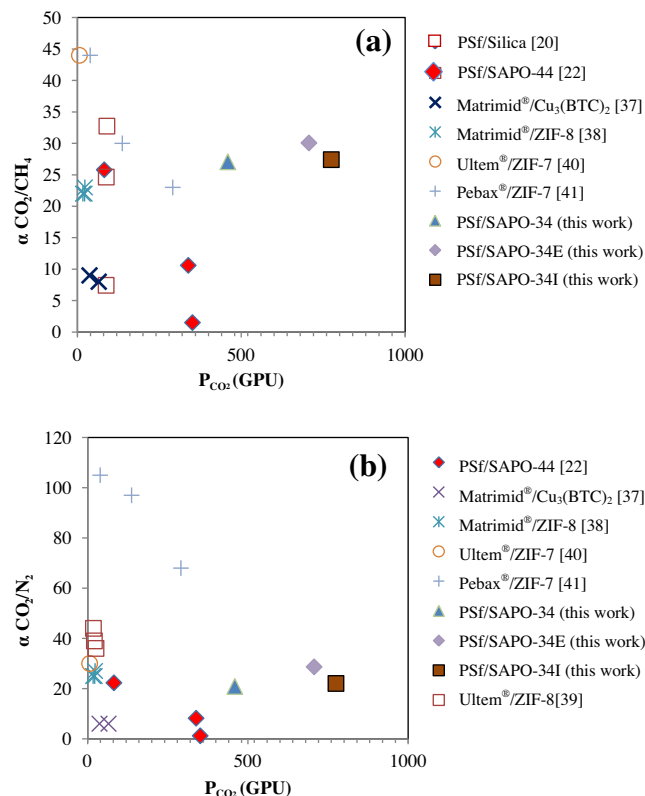

Fig. 7. Comparative study of the fabricated membranes in this work with asymmetric MMMs from literatures [20,22,36–40] (a) for CO_2/CH_4 and (b) for CO_2/N_2.

the silane coupling agent could also diminish the transportation of gases via the unselective voids as well [6]. The PSf/SAPO-34E MMM showed a great increment in CO_2 permeance and only relatively small growth in N_2 and CH_4 permeances compared to the PSf/SAPO-34 MMM with the same amount of filler. The selection of solvent in silane grafting is important as well as it resulted very different permeation data. Unlike the PSf/SAPO-34E MMM, the MMM containing SAPO-34I zeolite only exhibited slight improvement of CO_2 selectivity in gas separation compared to the MMM containing unmodified SAPO-34 zeolite. This variation between PSf/SAPO-34E and PSf/SAPO-34I membranes may be due to the difference in solvent polarity. Ethanol with polarity index of 5.2 could generate more uniform distribution of grafting site compared to IPA with polarity index of only 3.9. The utilization of a higher polar solvent in APMS grafting improved the mobility of silane molecules on the SAPO-34E surface, leading to not only less agglomeration, but also improve the adhesion between filler and PSf phases, which result to smaller interfacial voids formation [5,35].

The permeation results in this work were further compared with the recent works on asymmetric MMMs. The collected data and references were shown in Table 3. Fig. 7(a) and (b) were generated for direct comparison of gas performance. As shown in Fig. 7(a) and (b), both PSf/SAPO-34E and PSf/SAPO-34I MMMs showed significant higher CO_2 permeance than the asymmetric MMMs reported in the literature [20,22,36–40]. MMMs in this work also displayed satisfactory selectivity in CO_2/CH_4 and CO_2/N_2 after silane grafting of SAPO-34 zeolite. However, both APMS-treated PSf/SAPO-34E and PSf/SAPO-34I membranes possessed relatively low CO_2/N_2 selectivity as compared to Pebax®/ZIF-7 MMMs [40]. The distinction is due to the selection a glassy polymer in this work. Further modification of the polymer phase is hence suggested in the future work.

4. Conclusions

APMS was selected as the silane coupling agent instead of the other ethoxy group-based silane in this work because the methoxy group is more vulnerable to hydrolysis and it possesses less steric hindrance as compared to ethoxy group. The effects of using two different solvents, namely ethanol and IPA during the silane grafting reaction were studied. XRD patterns of both modified SAPO-34 samples showed the similar trend relative to unmodified SAPO-34 zeolite, but with reduction of intensity in certain range. BET analysis showed that APMS modification of SAPO-34 using ethanol caused an significant decrement in BET surface area of SAPO-34E compared to SAPO-34I with IPA as solvent. The changes in FTIR spectra of both modified SAPO-34 zeolite samples signified the successful reaction of APMS on the surface of SAPO-34 zeolite. More silane molecules were successfully reacted on the SAPO-34 zeolite surface using ethanol as solvent in the grafting reaction. However, all membrane samples possessed similar FTIR spectra and morphology as shown in SEM micrographs. Single gas permeation was carried out to investigate the effects of silane-grafting on the separation performance of these membranes. Both PSf/modified SAPO-34 membranes showed great enhancement in terms of selectivity and permeances relative to the pure PSf membrane in this work. The highest CO_2/N_2 and CO_2/CH_4 selectivities were detected in the PSf/SAPO-34E MMMs with the selectivity value increased to 28 (135% increment) and 31 (124% increment) respectively as compared to the pure PSf membrane. In addition, PSf/SAPO-34E MMMs possessed high CO_2 permeance of 706 GPU. The increment of CO_2 selectivity and permeance could be related to the well dispersion of SAPO-34 zeolite and the reduction of interfacial voids upon the introduction of the coupling agent into the system.

Acknowledgments

References

[1] R.S.C.P. Pandey, Prog. Polym. Sci. 26 (2001) 853–893.
[2] M. Peydayesh, S. Asarehpour, T. Mohammadi, O. Bakhtiari, Chem. Eng. Res. Des. (2013), http://dx.doi.org/10.1013/j.cherd.2013.01.022.
[3] U. Cakal, L. Yilmaz, H. Kalipcilar, J. Membr. Sci. 17–418 (2012) 45–51.
[4] D. Şen, H. Kalıpçılar, L. Yilmaz, J. Membr. Sci. 303 (2007) 194–203.
[5] X.Y. Chen, O.G. Nik, D. Rodrigue, S. Kaliaguine, Polymer 53 (2012) 3269–3280.
[6] A.F. Ismail, T.D. Kusworo, A. Mustafa, J. Membr. Sci. 319 (1–2) (2008) 306–312.
[7] T.W. Pechar, M. Tsapatsis, E. Marand, R. Davis, Desalination 146 (1–3) (2002) 3–9.
[8] T.W. Pechar, S. Kim, B. Vaughan, E. Marand, M. Tsapatsis, H.K. Jeong, C.J. Cornelius, J. Membr. Sci. 277 (1–2) (2006) 195–202.
[9] A.M.W. Hillock, S.J. Miller, W.J. Koros, J. Membr. Sci. 314 (1–2) (2008) 193–199.
[10] Y. Li, H.M. Guan, T.S. Chung, S. Kulprathipanja, J. Membr. Sci. 275 (1–2) (2006) 17–28.
[11] O.G. Nik, X.Y. Chen, S. Kaliaguine, J. Membr. Sci. 379 (1–2) (2011) 468–478.
[12] M.C. Brochier Salon, M.N. Belgacem, Phosphorus, Sulfur, Silicon Relat. Elem. 186 (2) (2011) 240–254.
[13] S. Li, J.L. Falconer, R.D. Noble, J. Membr. Sci. 241 (1) (2004) 121–135.
[14] J.Y. Lee, S.H. Lee, S.W. Kim, Mater. Chem. Phys. 63 (2000) 251–255.
[15] N.P. Damayanti, J. Sol-Gel Sci. Technol. 56 (1) (2010) 47–52.
[16] T.L. Chew, A.L. Ahmad, S. Bhatia, Chem. Eng. J. 171 (3) (2011) 1053–1059.
[17] J.Y. Kim, J. Kim, S.T. Yang, W.S. Ahn, Fuel 108 (2013) 515–520.
[18] O.G. Nik, M. Sadrzadeh, S. Kaliaguine, Chem. Eng. Res. Des. 90 (9) (2012) 1313–1321.
[19] G. Clarizia, C. Algieri, A. Regina, E. Drioli, Micropor. Mesopor. Mater. 115 (1–2) (2008) 67–74.
[20] M.F.A. Wahab, A.F. Ismail, S.J. Shilton, Sep. Purif. Technol. 86 (2012) 41–48.
[21] M.U.M. Junaidi, C.P. Leo, S.N.M. Kamal, A.L. Ahmad, T.L. Chew, Fuel Process. Technol. 118 (2014) 125–132.
[22] M.U.M. Junaidi, C.P. Leo, S.N.M. Kamal, A.L. Ahmad, T.L. Chew, Fuel Process. Technol. 112 (2013) 1–6.
[23] S. Balta, A. Sotto, P. Luis, L. Benea, B. Van der Bruggen, J. Kim, J. Membr. Sci. 389 (2012) 155–161.
[24] C.P. Leo, N.H. Ahmad Kamil, M.U.M. Junaidi, S.N.M. Kamal, A.L. Ahmad, Sep. Purif. Technol. 103 (2013) 84–91.
[25] M.A. Aroon, A.F. Ismail, M.M. Montazer-Rahmati, T. Matsuura, Sep. Purif. Technol. 72 (2) (2012) 194–202.
[26] T.H. Young, L.W. Chen, Desalination 103 (3) (1995) 233–247.
[27] J. Han, W. Lee, J.M. Choi, R. Patel, B.R. Min, J. Membr. Sci. 351 (1–2) (2010) 141–148.
[28] A.F. Ismail, P.Y. Lai, Sep. Purif. Technol. 33 (2) (2003) 127–143.
[29] D. Wang, K. Li, W.K. Teo, J. Membr. Sci. 115 (1) (1996) 85–108.
[30] A. Mansourizadeh, A.F. Ismail, J. Membr. Sci. 348 (1–2) (2010) 260–267.
[31] F. Dorosti, M.R. Omidkhah, M.Z. Pedram, F. Moghadam, Chem. Eng. J. 171 (3) (2011) 1469–1476.
[32] P. Jha, J.D. Way, J. Membr. Sci. 324 (1–2) (2008) 151–161.
[33] Y. Zhang, K.J. Balkus Jr., I.H. Musselman, J.P. Ferraris, J. Membr. Sci. 325 (1) (2008) 28–39.
[34] Y.C. Hudiono, T.K. Carlisle, A.L. LaFrate, D.L. Gin, R.D. Noble, J. Membr. Sci. 370 (1–2) (2011) 141–148.
[35] O.G. Nik, B. Nohair, S. Kaliaguine, Micropor. Mesopor. Mater. 143 (1) (2011) 221–229.
[36] J. Hu, H. Cai, H. Ren, Y. Wei, Z. Xu, H. Liu, Y. Hu, Ind. Eng. Chem. Res. 49 (24) (2010) 12605–12612.
[37] S. Basu, A. Cano-Odena, I.F.J. Vankelecom, Sep. Purif. Technol. 81 (1) (2011) 31–40.
[38] Y. Dai, J.R. Johnson, O. Karvan, D.S. Sholl, W.J. Koros, J. Membr. Sci. 401–402 (2012) 76–82.
[39] S. Husain, W.J. Koros, J. Membr. Sci. 288 (1–2) (2007) 195–207.
[40] T. Li, Y. Pan, K.V. Peinemann, Z. Lai, J. Membr. Sci. 425–426 (2013) 235–242.